

Loop I/NPS morphology predictions in the ultralong-wavelength band

YANPING CONG,¹ BIN YUE,^{2,3} YIDONG XU,^{2,3} FUREN DENG,^{2,4} JIAJUN ZHANG,¹ AND XUELEI CHEN^{2,3,4}

¹*Shanghai Astronomical Observatory, Chinese Academy of Sciences, Shanghai 200030, China*

²*National Astronomical Observatories, Chinese Academy of Sciences, 20A Datun Road, Chaoyang District, Beijing 100101, China*

³*Key Laboratory of Radio Astronomy and Technology, Chinese Academy of Sciences, 20A Datun Road, Chaoyang District, Beijing 100101, China*

⁴*School of Astronomy and Space Science, University of Chinese Academy of Sciences, Beijing 100049, China*

ABSTRACT

Loop I/North Polar Spur (NPS) is the giant arc structure above the Galactic plane observed at radio wavelengths ($\lesssim 10$ GHz). There has been long-standing debate about its origin. While many people believe that it consists of nearby supernova remnants (SNRs), some others consider it as a giant bubble close to the Galactic Center (GC), associated with the Fermi Bubble and the eROSITA X-ray bubble. At ultra-long wavelengths (wavelength $\gtrsim 10$ m or frequency $\lesssim 30$ MHz), particularly below ~ 10 MHz, the free-free absorption of the radio signal by diffuse electrons in the interstellar medium (ISM) becomes significant, resulting in different sky morphologies from those at higher frequencies. In this paper, we develop emissivity models for the two Loop I/NPS origin scenarios, and predict the Loop I/NPS morphology at ultra-long wavelengths in both scenarios, taking into account the free-free absorption effect. We find that in the SNRs model, the full Loop I/NPS will still be a bright arc even at ~ 1 MHz. In the GC model, the arc is fully visible only above ~ 3 MHz. While below this frequency, it is visible only at Galactic latitudes $b \gtrsim 30^\circ$; the $b \lesssim 30^\circ$ part becomes invisible due to the absorption by the ISM electrons between the GC and the Sun. The upcoming space missions aiming at ultra-long wavelengths, such as the DSL and the FARSIDE, can potentially distinguish these two scenarios and provide decisive information about the origin of the Loop I/NPS.

Keywords: Interstellar medium (847) — Interstellar plasma (851) — Interstellar absorption (831) — Milky Way Galaxy (1054) — Radio interferometers (1345)

1. INTRODUCTION

In radio bands, Loop I exhibits a conspicuous giant loop-like (arc) feature above the Galactic plane in the sky (Baldwin 1955; Roger et al. 1999; Dowell et al. 2017; Eastwood et al. 2018; Guzmán et al. 2011; Landecker & Wielebinski 1970; Patra et al. 2015; Haslam et al. 1982; Reich & Reich 1986; Intema et al. 2017), covering an area of $\sim 70^\circ \times 50^\circ$ (Lallement 2023). It crosses the Galactic plane at Galactic longitude $l \sim 30^\circ$ and Galactic latitude $b \sim 10^\circ$, and extends toward the north Galactic pole to about $l \sim 330^\circ$ and $b \sim 80^\circ$. There is also a bright spur near the root of Loop I (Hanbury Brown et al. 1960), named North Polar Spur (NPS, e.g. Iwashita et al. 2023). In this paper, we use “Loop I/NPS” to refer to the full loop-like structure. In the soft X-ray band, there is also a loop-like structure above the Galactic plane, which coincides largely with the radio Loop I/NPS (Egger & Aschenbach 1995). The X-ray structure is quasicircular and is generally identified as a bubble, i.e. the northern eROSITA bubble. Below the Galactic plane, there is the southern eROSITA bubble that is roughly symmetric to its sibling (Predehl et al. 2020). However, in the radio bands, no corresponding structure was found in the total intensity map.

Besides the Loop I/NPS, other loop-like structures have also been found and designated as Loop II (Cetus arc) (Large et al. 1962), Loop III (Quigley & Haslam 1965), and Loop IV (Large et al. 1966; Berkhuijsen et al. 1971), respectively. The Loop I structure, and many other smaller and dimmer loop-like structures, are highly polarized

(Planck Collaboration et al. 2016a). The polarized structure of Loop I seems to extend far below the Galactic plane (Vidal et al. 2015; Panopoulou et al. 2021).

The debate on the origin of the Loop I/NPS structure, including its position and physical size, has persisted for over ~ 40 years and remains contentious (e.g. Dickinson 2018; Planck Collaboration et al. 2016a; Kataoka et al. 2018; Shchekinov 2018). Because of its huge angular size ($\sim 120^\circ$, Dickinson 2018), many people consider it to be a nearby object within $\lesssim 1$ kpc, but the exact distance and geometry are still uncertain. One method for deriving the distance of the Loop I/NPS is to analyze the alignment between the polarization angles of the optical starlight and the synchrotron in the same direction. These two angles should be highly correlated with each other if the synchrotron radiation comes from sources closer than the stars, since the starlight polarization is expected to be generated by dust that traces the magnetic field, which also produces the synchrotron. Moreover, the thermal dust emission polarization also traces the magnetic field. Panopoulou et al. (2021) analyzed the polarization angles of these three tracers and derived upper limits on the Loop I/NPS distance, being all below ~ 150 pc. It strongly favors that the Loop I, at least the part at $b > 30^\circ$, is a nearby source. Some authors suggested that it is a superbubble neighboring the Local Hot Bubble (LHB) where we reside (Cox & Reynolds 1987), created by stellar winds and a series of supernova explosions happened in recent several million years in the Scorpius–Centaurus OB association that is ~ 170 pc away from the Sun (de Geus 1992; Breitschwerdt & de Avillez 2006). The Geminga pulsar was produced in one of these supernova explosions (Burke et al. 2019). It was further pointed out that the Loop I/NPS superbubble is interacting with the LHB where we reside, and the interaction zone forms a dense HI ring (wall) between those two bubbles. The existence of the dense HI ring is supported by the sudden increase of HI column density at ~ 40 pc from Sun, indicated by the optical and UV absorption spectra of stars toward the center of the Loop I/NPS (Centurion & Vladilo 1991); the coherence of X-ray absorption shadow and the HI column density distribution (Egger & Aschenbach 1995), and the strengthened intensity of far-UV OVI emission line (Sallmen et al. 2008).

On the other hand, Reis & Corradi (2008) analyzed the color excess of more than 4000 stars up to 500 pc from the Sun, and Santos et al. (2011) analyzed the optical polarization of more than 800 stars. They found that the interface between the Loop I/NPS and the LHB is fragmented and distorted. Such a discovery questions the notion of a coherent ring structure formed by the interaction of the Loop I/NPS with the LHB. Moreover, the analysis of X-ray absorption by the gas between the Loop I/NPS and the Sun indicates that the Loop I/NPS could be more distant, about $\sim 500 - 1000$ pc away (Iwan 1980; Sofue 2015; Lallement et al. 2018). Faraday rotation depolarization and Faraday tomography methods also favour a distance of several hundred pc for the Loop I/NPS; see reviews Dickinson (2018) and Lallement (2023), and references therein.

Some people instead propose that the Loop I/NPS may originate from the Galactic Center (GC) (Sofue et al. 1974; Sofue 2000), based on its directional proximity and possible association with the eROSITA bubble in the X-ray band, and with the Fermi Bubble in the gamma-ray band (Su et al. 2010; Predehl et al. 2020). Both the eROSITA bubble and the Fermi bubble are roughly symmetric with respect to the Galactic plane, strongly favoring the GC hypothesis (Sofue 1977, 2000; Sofue et al. 2016). In such a scenario, since the structure is located at ~ 8 kpc away, it must have considerable physical size (Sarkar 2019; Sofue 1977, 1994). Using morphology analysis, Liu et al. (2024) also proposed that the NPS/eROSITA bubble is a distant and giant structure close to the GC. Sofue (2017) measured the HI gas density in the inner Milky Way, and found that there is an HI hole around the GC, and the hole has a crater-shaped wall that coincides with the Loop I/NPS. Zhang et al. (2024) investigated the distance to the polarized radio counterparts, including the Loop I/NPS, of the eROSITA bubbles by analyzing the multi-wavelength Faraday rotation depolarization. The wavelength-dependent depolarization reveals that the magneto-ionic medium responsible for the observed depolarization must extend up to a distance of 5 kpc. This finding suggests a connection between the polarized Loop I/NPS and outflows originated from the GC. The GC origin hypothesis is also supported by the fact that the measured H α -to-1.4 GHz radio intensity ratio for the Loop I/NPS is two orders of magnitude smaller than the typical shell-type SNRs (Sofue et al. 2023). The North-South asymmetry is explained by the lower density of the medium in the southern hemisphere. Expansion in a low-density medium results in weak shock acceleration efficiency, and hence weak radiation (Lallement 2023; Sarkar 2019).

In the radio band, Loop I/NPS's emission is mainly the synchrotron radiation (Borka 2007). There have been many models developed to explain the Loop I/NPS's morphology. In the supernova remnants (SNRs) scenario, the bright ridge originates from a compressed magnetic field and/or enhanced cosmic ray, i.e., the emissivity at the shell is larger than the interior. The asymmetry of the loop is due to the inhomogeneous distribution of the gas (see Dickinson 2018 and references therein). In the ultra-long wavelength band (wavelength $\gtrsim 10$ m or frequency $\lesssim 30$ MHz), particularly

at frequencies $\lesssim 10$ MHz, the free-free absorption by diffuse electrons in the interstellar medium (ISM) becomes important and may change the observed morphology of the radio sky, including the Loop I/NPS structure (Cong et al. 2021, 2022). The Loop I/NPS, at least the low Galactic latitude part, is expected to be darker if it is located at the GC, but will still be bright if it is a complex of nearby SNRs. Cong et al. (2021) pointed out that the ultra-long wavelength observations have the potential to solve the problems of Loop I/NPS's origin. In this paper, we explicitly investigate this problem. We develop phenomenological models to predict the observational features of the Loop I/NPS for both the SNRs scenario and the GC scenario, in the ultra-long wavelength band. The outline of this paper is as follows. In Sec. 2, we present the emissivity model for the Galactic disk and the Loop I/NPS structure in these two scenarios. Then we develop an electron density model for the Loop I/NPS. The main results and discussion on some uncertainties are presented in Sec. 3. We summarize the results in Sec. 4

2. METHODS

In this work, we model the Galactic emissivity as comprising of a smooth disk component, including both the thin and thick disks¹, and a Loop I/NPS structure. Model parameters are derived by reproducing the observed Haslam 408 MHz all-sky map (Haslam et al. 1982; Remazeilles et al. 2015), and extrapolated to lower frequencies by a power-law formula.

2.1. The disk emissivity

We assume that the Galactic disk synchrotron emissivity is composed of a thin disk component and a thick disk component. The thin disk is geometrically thin but dominates the Galactic plane and around. It is associated with star formation, regular magnetic field and SNRs around Galactic spiral arms. The thick disk is more extended in the vertical direction and dominates the emission at high Galactic latitudes. It reflects the transport and diffuse processes of cosmic rays, and both random and regular Galactic halo magnetic fields (e.g. Mertsch & Sarkar 2013; Jansson & Farrar 2012; Sun et al. 2008). As for the radiation from the Loop I/NPS and its vicinity, the contribution from both high latitudes and low latitudes is important, it is necessary to model both of them. Although this two-disk scenario has not yet been confirmed in observations, we find that it fits the 408 MHz sky map better than the one-disk model adopted in Cong et al. (2021).

The disk emissivity can be written as

$$\epsilon_{\text{disk}}(\nu|R, Z) = \sum_i A_i \exp \left\{ -b(\alpha_i) \left[\left(\frac{R}{R_i} \right)^{\frac{1}{\alpha_i}} - 1 \right] \right\} \operatorname{sech} \left(\frac{Z}{Z_i} \right) \left(\frac{\nu}{\nu_*} \right)^{\beta_G}, \quad (1)$$

where $i \in [\text{thin, thick}]$. R and Z are cylindrical Galactic coordinates, where R is the radial distance to the GC, while Z is the vertical distance to the Galactic plane. Here ν is the frequency, and β_G is the spectral index. The radial dependence form of Eq. (1) is the Sérsic profile (Sersic 1968) that is widely used to fit the surface brightness distribution of elliptical galaxies, as well as the disk and bulge components of other galaxy types. A_i denotes the emissivity at the effective radius R_i , which encompasses half of the total intensity in $Z = 0$ plane. The index α_i indicates the profile's curvature in the radial direction. Z_i is the height scale. Finally, the function $b(\alpha)$ is a dimensionless scale factor. It is the solution to

$$\Gamma(2\alpha, b) = 2 \int_0^b t^{2\alpha-1} e^{-t} dt, \quad (2)$$

where Γ is the Gamma Function. We use the following approximation (Ciotti & Bertin 1999; MacArthur et al. 2003)

$$b(\alpha) = \begin{cases} 0.01945 - 0.8902\alpha + 10.95\alpha^2 - 19.67\alpha^3 + 13.43\alpha^4 & \alpha \leq 0.36 \\ 2\alpha - \frac{1}{3} + \frac{4}{405\alpha} + \frac{46}{25515\alpha^2} + \frac{131}{1148175\alpha^3} + \frac{2194697}{30690717750\alpha^4} & \alpha > 0.36. \end{cases} \quad (3)$$

The frequency-independent parameters A_i , R_i , α_i , and Z_i , together with the parameters in the Loop I/NPS emissivity model to be introduced in Sec. 2.2, are obtained by fitting the Haslam 408 MHz map (Haslam et al. 1982; Remazeilles et al. 2015), for which the free-free emission and the isotropic extragalactic radiation are pre-subtracted. The fitted

¹ It is worth noting that this is not the same concept as the optical thin disk and thick disk; these thin and thick disks describe the diffuse components in radio bands, primarily originating from synchrotron radiation.

parameters of both the disk component and the Loop I/NPS component are given in Tab. 1. When pre-processing the Haslam 408 MHz map, the free-free emission can be derived from the H α emission line. However, there are uncertainties induced by dust absorption and scattering at the Galactic plane and in some dense HII regions (e.g. Dickinson et al. 2003). We derive the frequency-dependent free-free sky maps from the emission measure (EM) and electron temperature sky maps provided by Planck Collaboration et al. (2016b), taking into account the free-free self-absorption. The formulae are listed in Eq. (14) of Cong et al. (2021). The free-free sky map at 408 MHz and the global spectrum are shown in Fig. 2 of that paper. At 408 MHz, for high Galactic latitude regions with $|b| \gtrsim 10^\circ$, free-free emission only contributes $\sim 1\%$ to the total intensity. Due to the shallower spectrum index compared with synchrotron ($\beta_{ff} \sim -2.1$ for free-free emission vs. $\beta_G \sim -2.5$ for synchrotron), this contribution becomes even negligible below ~ 10 MHz. Free-free emission is highly concentrated on the Galactic plane. In some particularly dense HII regions (for example, the dense HII regions in Orion-Eridanus Superbubble, Perseus-Taurus Supershell, and Ophiuchus Superbubble), the free-free model would be inaccurate. It may underestimate the free-free emission and absorption. However, the present work focuses on the Loop I/NPS and regions around it; this is large-scale morphology, and such flaws will not change our conclusions. We model the extragalactic background as isotropic radiation, $T_{eg} = 1.2(\frac{\nu}{1\text{GHz}})^{-2.58}$, derived from ARCADE-2 observations (Seiffert et al. 2011).

Throughout this paper, we use a constant spectrum index, $\beta_G = -2.51$, for Galactic synchrotron emissivity (Cong et al. 2021). This value is derived by fitting the observed sky maps at 10 frequencies from 35 MHz to 408 MHz (Dowell et al. 2017; Guzmán et al. 2011; Haslam et al. 1982; Remazeilles et al. 2015).

2.2. The Loop I/NPS emissivity

No matter whether the Loop I/NPS is a superbubble created by stellar winds or supernova explosion shocks, or is a giant bubble located at the GC and created by outflows associated with star formation/black hole activities, the ambient medium is swept and compressed, and it must finally form a cavity with a dense shell. The shell could be incomplete or asymmetric if the medium is inhomogeneous. Motivated by this, we begin by modeling the Loop I/NPS emissivity as a sphere with a thin and dense spherical shell, which we then trim to reproduce the observed loop morphology. Similar scenarios have been extensively employed in studies of radio loop morphology (e.g. Wolleben 2007; Mertsch & Sarkar 2013; Mou et al. 2023a). Let the radius of the sphere be r_L and the thickness of the shell be Δr_s , then the emissivity of the Loop I/NPS can be written as:

$$\epsilon_L(r) = \begin{cases} \epsilon_i & r < r_L - \Delta r_s \\ \epsilon_s & r_L - \Delta r_s \leq r \leq r_L \\ 0 & r > r_L, \end{cases} \quad (4)$$

where ϵ_i is the emissivity of the sphere's interior, ϵ_s is the emissivity of the shell, and r is the distance to the center of the Loop I/NPS sphere. Given that $\epsilon_s \gg \epsilon_i$, the projection of the sphere onto the celestial sphere results in a limb-brightened loop. By adjusting the sphere's radius, the shell thickness, and its emissivity, and by selecting which part of the shell to trim, the model can accurately reproduce the observed bright Loop I/NPS arc.

In this study, we examine two potential scenarios for the origin of Loop I/NPS: the shell-like SNRs model, which attributes the Loop I/NPS to supernova remnants near the Sun; and the GC model, which places the Loop I/NPS close to the center of the Milky Way, akin to the Fermi Bubble. For both models, the angular size of the Loop I/NPS is approximately $\sim 116^\circ$ (Mertsch & Sarkar 2013), implying a large difference in its physical size.

2.2.1. The shell-like SNRs model

In this model, we adopt the direction (the Galactic longitude and latitude) of the Loop I/NPS center and its distance to the Sun given in Berkhuijsen et al. (1971); Mertsch & Sarkar (2013), i.e., the center of the Loop I/NPS sphere is at Galactic Cartesian coordinates ($X_L = -8.3$, $Y_L = -0.12$, $Z_L = 0.07$) kpc. The observed morphology of the Loop I/NPS exhibits irregular characteristics. This is likely a result of the interaction between supernova remnants and a joint envelope formed by the stellar winds of the Sco-Cen OB association or the LHB (Egger & Aschenbach 1995; Vidal et al. 2015). Thus, it is necessary to eliminate certain portions of the emissivity sphere to reproduce the observed morphology accurately.

We first remove the portion of the Loop I/NPS below the Galactic plane, $Z < 0$, to address the north-south asymmetry. Then we create a suppositional 3D ellipse centred at Galactic Cartesian coordinates ($X = -8.522$, $Y =$

$-0.089, Z = 0.029$) kpc with axes of $(2r_L, 0.4r_L, 2r_L)$, and remove the volume in the Loop I/NPS overlaps with this ellipse. This is motivated by the east-west asymmetry in the observed morphology. Following this processing, we successfully produce the morphological features of the Loop I/NPS as observed in the Haslam 408 MHz map.

2.2.2. The Galactic Center model

In the GC model, the Loop I/NPS is considered as the post-shock medium (Mou et al. 2023a). The center of the sphere is at Galactic Cartesian coordinates $(X_L = 0.0, Y_L = 1.5, Z_L = 5.0)$ kpc. It consistently aligns with the shape of the Fermi Bubble and the X-ray Bubble (Mou et al. 2023b). Similar to the shell-like SNRs model, here we also remove the portion where $Z < 0$. However, in the GC model, the $Z < 0$ portion is a small fraction compared to its northern counterpart because now the center of the Loop I/NPS is well above the Galactic plane. Then we create a suppositional sphere in 3D space centered at Galactic Cartesian coordinates $(X_L = -5.262, Y_L = -5.608, Z_L = 1.142)$ kpc with a radius of r_L and eliminate the overlap between the Loop I/NPS and the sphere to address the east-west asymmetry.

Table 1. The frequency-independent parameters for the thin and thick disks and the Loop I/NPS emissivity, in the SNRs and GC models for the Loop I/NPS, derived by fitting the observed 408 MHz Haslam sky map after extracting the free-free emission and the extragalactic background. It is natural that in both the SNRs and GC models of the Loop I/NPS, the parameters for disks are close to each other. X_L , Y_L , and Z_L are the assigned Galactocentric Cartesian coordinates of the Loop I/NPS center.

Disk parameters	in the SNRs model	in the GC model
A_{thick} (K/kpc)	1.65	1.73
R_{thick} (kpc)	5.67	5.73
α_{thick}	0.15	0.14
Z_{thick} (kpc)	3.04	2.80
A_{thin} (K/kpc)	5.01	5.0
R_{thin} (kpc)	7.82	8.30
α_{thin}	1.94	2.09
Z_{thin} (kpc)	0.3	0.3
Loop I/NPS parameters		
X_L (kpc)	-8.3	0.0
Y_L (kpc)	-0.12	-1.5
Z_L (kpc)	0.07	5.0
r_L (kpc)	0.22	7.8
Δr_s (kpc)	0.02	2.5
ϵ_s (K/kpc)	129.68	1.37
ϵ_i (K/kpc)	0.001	0.26

Finally, the total emissivity of the Milky Way is the sum of emissivities of the thin disk, the thick disk, and the Loop I/NPS,

$$\epsilon_{\text{MW}}(\nu|R, Z) = \epsilon_{\text{disk}}(\nu|R, Z) + \epsilon_{\text{L}}(\nu|R, Z). \quad (5)$$

We then fit the observed 408 MHz sky map (free-free emission and extragalactic background subtracted) with Eq. (5) (the coordinates of the Loop I/NPS center are specified in each model). The parameters derived for the thin and thick disks, as well as for the Loop I/NPS, are listed in Tab. 1. When the adopted Loop I/NPS model switches from SNRs to GC, we always obtain consistent parameters for the disk. It is interesting to note that, our Z_{thin} is roughly consistent with the observed optical thin disk which contains younger stars, gas, and dust with a scale height of $\sim 120 - 300$ pc; although our Z_{thick} is a bit larger than the scale height of optical thick disk (typically $\sim 0.5 - 1.9$ kpc) that contains elder stars (see Vieira et al. 2023 and references therein).

Fig. 1 shows the emissivity distribution slices of the Milky Way, encompassing both the disk and the Loop I/NPS in the two models. We obtain the sky map by integrating this emissivity along each line-of-sight and show the results at 408 MHz in Fig. 2. Our emissivity models replicate the morphology of the observed sky map very well.

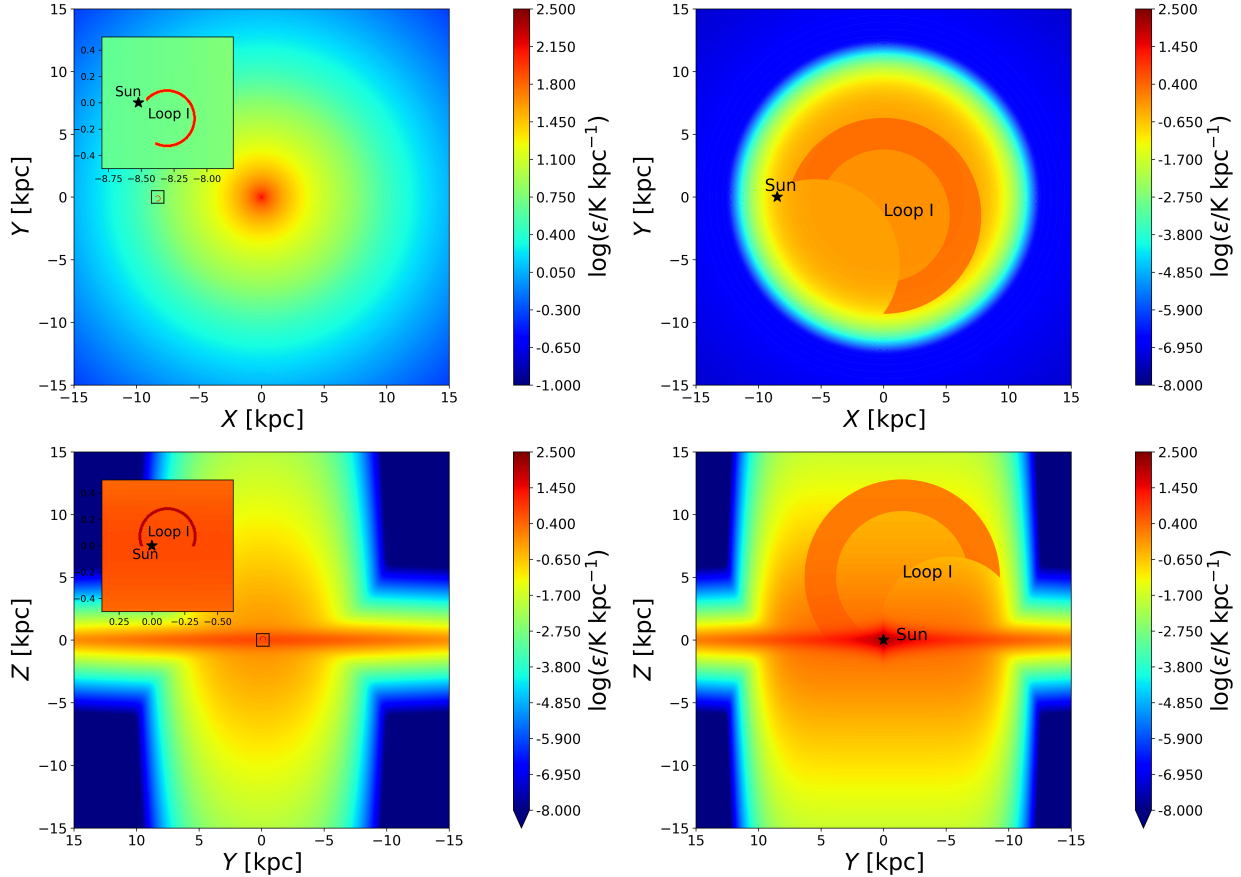


Figure 1. Emissivity distributions at 408 MHz in Galactocentric coordinates for the two models of the Loop I/NPS: shell-like SNRs (left) and GC (right). The slices are in the $X - Y$ plane (face-on, top), and the $Y - Z$ plane (edge-on, bottom), respectively.

2.3. The electron density of the Loop I/NPS

In order to model the free-free absorption by electrons at the ultra-long wavelengths, we adopt the NE2001 model for Galactic free electron distribution (Cordes & Lazio 2002, 2003). It comprises five components: the smooth component comprising the thin and thick disks and five spiral arms, the Galactic Center, the local interstellar medium including a few nearby voids, a list of known dense clumps, and a list of more distant voids. In the NE2001 model, the Loop I/NPS is one of the nearby voids in the local interstellar medium, manifesting a hemisphere void above the Galactic plane, with a thin shell. In this work, we improve the Loop I/NPS structure in the electron density model. We assume that the geometry of the Loop I/NPS is the same as the emissivity model, but derive the electron densities from **HaloSat** X-ray observations (LaRocca et al. 2020a).

HaloSat is a satellite designed to detect diffuse X-ray emissions in the range 0.4 - 7.0 keV (Kaaret et al. 2019; LaRocca et al. 2020b). It has a full response field-of-view of 10° , which makes it a useful tool for probing the thermal X-ray emission from the Loop I/NPS free electrons. **HaloSat** provides 14 pointing directions for the Loop I/NPS region. LaRocca et al. (2020a) proposed that the Loop I/NPS consists of a two-phase plasma: a cool component with an average energy of 0.087 keV (temperature $\sim 1.01 \times 10^6$ K) and a hot component with an average energy of 0.274 keV (temperature $\sim 3.18 \times 10^6$ K)². Both of them are optically thin and in ionization equilibrium. They fitted the EM values of the two components of the Loop I/NPS for the 14 pointing directions according to the observed X-ray spectra. The value of EM decreases with the increase in angle relative to the GC. We sum the EM for the cool and hot components to obtain the full EM for the Loop I/NPS. In principle, if the Loop I/NPS is an unknown structure

² LaRocca et al. (2020a) supposes that the Loop I/NPS fully contribute to the fitted hot component, and primarily contribute to the fitted cool component.

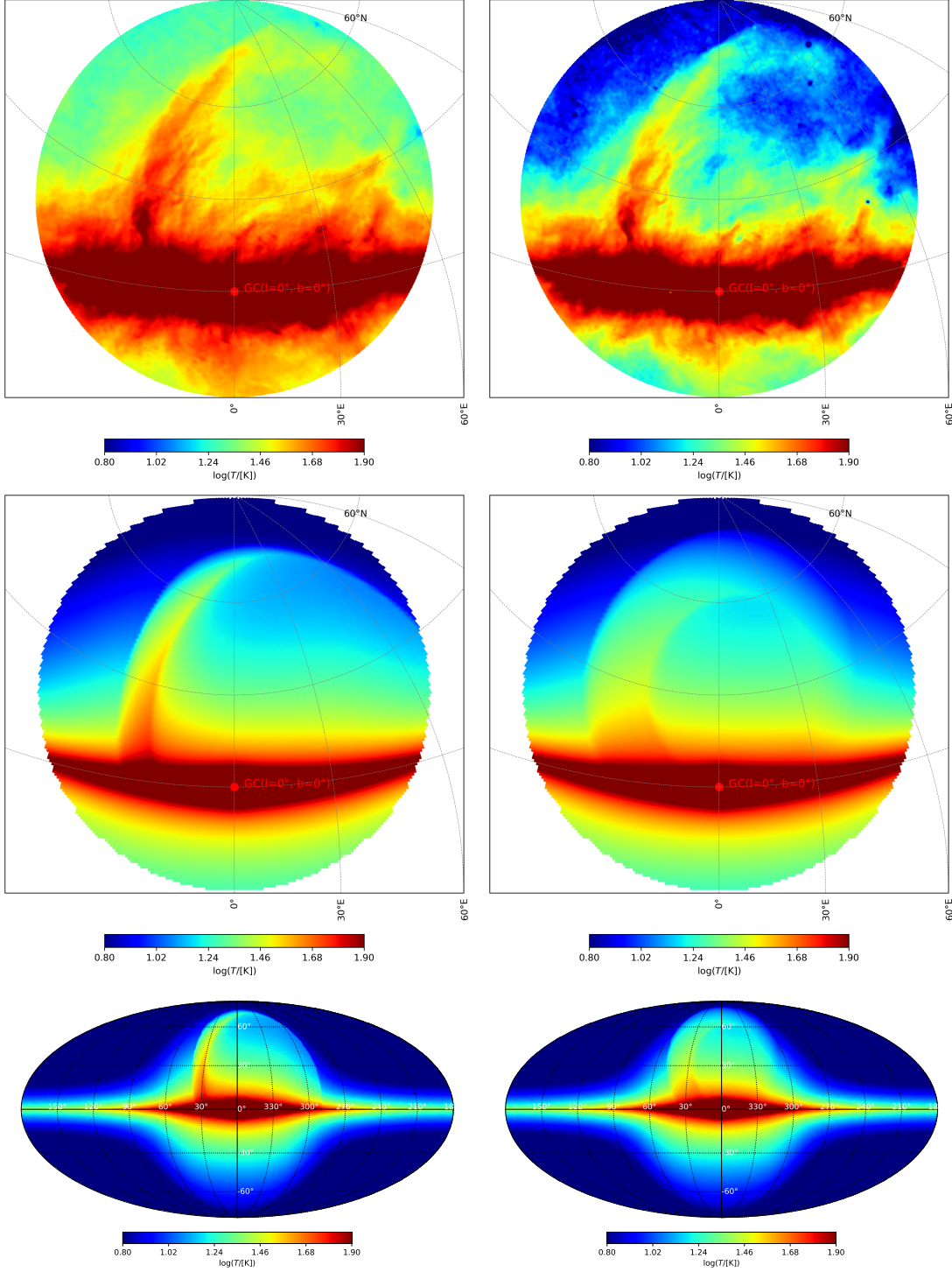


Figure 2. *Top left:* The Loop I/NPS structure and its vicinity in raw Haslam 408 MHz sky map, viewed in stereographic projection. *Top right:* Similar to top left panel, however the free-free emission and extragalactic background have been subtracted. *Middle left:* Our predicted Loop I/NPS and its vicinity at 408 MHz in stereographic projection, for the SNRs model. *Middle right:* Similar to the middle left panel, but the GC model for Loop I/NPS is adopted. *Bottom left:* The predicted full sky map at 408 MHz, including both the disk and the Loop I/NPS, in Mollweide projection, for the SNRs model. *Bottom right:* Similar to the bottom left panel, but for the GC model. All predicted sky maps do not include free-free emission and extragalactic background. The maps are displayed in Galactic coordinates, and the color scale uses a logarithmic stretch to better display the full model, particularly for regions away from the Galactic plane.

at the GC, the observed EM is from both the Loop I/NPS and the ISM in-between. However, since the emissivity of the Loop I/NPS dominates over the intervening ISM in the radio sky, here we naively assume the measured EM is also mainly from the Loop I/NPS.

For the i -th line-of-sight, the EM of the Loop I/NPS is

$$\text{EM}_i = \sum_{j=1}^{N_i} \frac{1}{f_e} n_{e,j}^2 \Delta s_{i,j}, \quad (6)$$

where this line-of-sight passes N_j segments in the Loop I/NPS. For the j -th segment, the electron density is $n_{e,j}$, and the path length is $\Delta s_{i,j}$. f_e is a filling factor and we use $f_e = 0.5$ (LaRocca et al. 2020a).

We divide the spherical coordinates θ of the Loop I/NPS-centered frame sphere shell into 20 parts and ϕ coordinates into 4 parts, where θ is the polar angle and ϕ is the azimuthal angle in the regular spherical coordinate system. The interior of the sphere is a single part with uniform density. We then perform Markov Chain Monte Carlo (MCMC, Foreman-Mackey et al. 2013) fitting for all the 14 line-of-sights in `HaloSat` observations, to find the electron density for each segment. For the segment without any line-of-sight passing, the electron density is assigned by interpolation from the nearest segment.

Fig. 3 shows the constructed electron density distribution of the Loop I/NPS for the slices of $X' = 0$, $Y' = 0$, and $Z' = 0$ in the Loop I/I/NPS-centered coordinate frame. The EM is converted into optical depth via (Condon & Ransom 2016)

$$\tau_\nu \approx 3.28 \times 10^{-7} \left(\frac{T_e}{10^4 \text{ K}} \right)^{-1.35} \left(\frac{\nu}{\text{GHz}} \right)^{-2.1} \left(\frac{\text{EM}}{\text{pc cm}^{-6}} \right), \quad (7)$$

assuming electron temperature $T_e = 10^6$ K, for the two Loop I/NPS models. The optical depth for free-free absorption of the Loop I/NPS solely at 1 MHz is presented in Fig. 4. Interestingly, the optical depth maps do not show loop-like features, which is consistent with the EM map derived from Planck observations (Planck Collaboration et al. 2020). As a comparison, in Fig. 4 we also show the integrated free-free optical depth for the full Milky Way, including the contribution of the Loop I/NPS and other Galactic electrons. Compared with this total optical depth, the contribution from the Loop I/NPS is negligible and invisible on the maps.

We find that, the optical depth from the Loop I/NPS itself is small, primarily because the electrons therein are hot. The EM derived from `HaloSat` observations is for electrons with temperature $\sim 10^6$ K, much hotter than the typical WIM (several thousand K) in the Milky Way. However, it seems that in the Loop I/NPS, electrons with temperature close to the typical WIM are few because in the H α sky map, there is no corresponding loop-like structure found (Haffner et al. 2003). We check that, if we replace the Loop I/NPS model with a hemisphere with a radius of 7.8 kpc (0.22 kpc), the thickness of the shell 2.5 kpc (0.02 kpc), density of the shell 0.01 cm^{-3} (0.081 cm^{-3}) and density of the sphere interior 0.005 cm^{-3} (0.024 cm^{-3}), and temperature 10^6 K. The optical depth is still always lower than $\sim 3 \times 10^{-3}$. If the temperature is set to be 8000 K, then the optical depth can reach up to ~ 2 , reducing the radiation behind Loop I/NPS to $\sim 14\%$. In summary, the self-absorption of the Loop I/NPS emission should have modest effects on the final sky map.

3. RESULTS AND DISCUSSION

3.1. Results

With the modeled 3D emissivity and free electron distribution, the sky map is obtained by performing integration of the radiative transfer function along each line-of-sight. Considering the free electron distribution within the Milky Way, radiation from the Loop I/NPS would experience absorption in the ultra-long wavelength band. If the Loop I/NPS is a complex of nearby SNRs, the absorption between Loop I/NPS and the observer would be small; whereas if it is located near the GC, the influence of absorption by the ISM would be significant. Our calculations validate these expectations. In Fig. 5 we present the predicted sky maps at frequencies 10, 3, and 1 MHz, respectively, for our two Loop I/NPS origin models. Clearly, below ~ 10 MHz, particularly at the frequency as low as 1 MHz, the high Galactic latitude regions are brighter while the Galactic disk is darker. However, In Fig. 5, on the Galactic disk, at the directions where the projection of electron density is low in the NE2001 model, say the LDR (low-density region, $30^\circ \lesssim l \lesssim 90^\circ$) and the LSB (local superbubble around $l \sim 240^\circ$), there are bright patches. This is already pointed out in Cong et al. (2021).

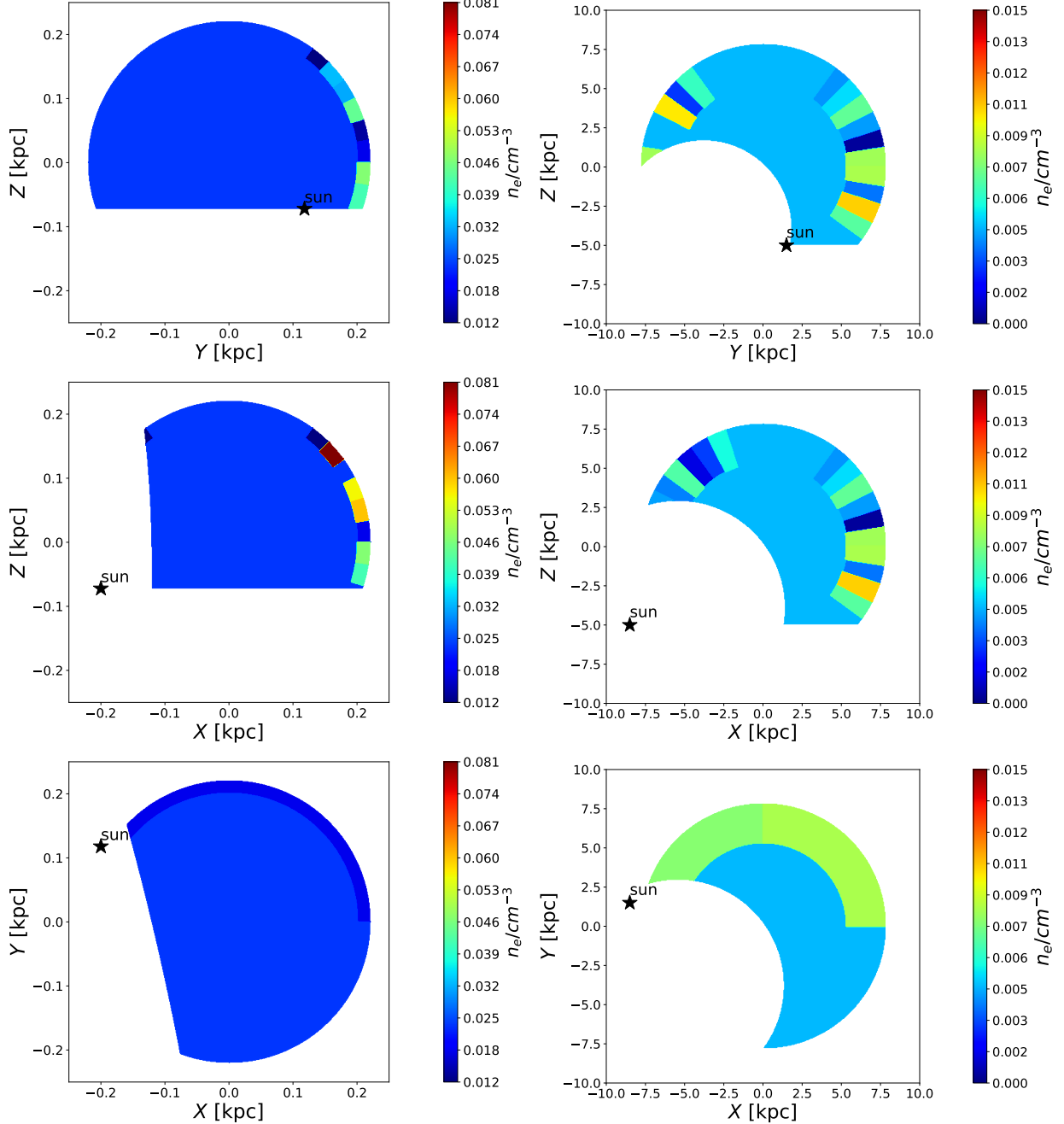


Figure 3. The Loop I/NPS electron density constructed from `HaloSat` observations for the shell-like SNRs (left) and GC model (right), respectively. From top to bottom, we plot the $X' = 0$, $Y' = 0$, and $Z' = 0$ planes, respectively, in the Loop I/NPS-centered coordinate frame and mark the Sun’s position of the projection in each panel. In the left panels, the Sun’s position is at $(-0.196, 0.118, -0.072)$ kpc, while in the right panels, it is at $(-8.5, 1.5, -5)$ kpc.

At frequencies $\gtrsim 3$ MHz, in both shell-like SNRs and GC models, the Loop I/NPS still appears as a bright arc. But there are differences at frequencies as low as ~ 1 MHz. The full Loop I/NPS is still a bright structure in the shell-like SNRs model. This is because it is very close to the observer, and the absorption by the ISM electrons is negligible. However, in the GC model, the morphology is quite different. The Loop I/NPS disappears at $b \lesssim 30^\circ$, due to the absorption of electrons between the GC and the observer. So indeed, the ultra-long wavelength observations can distinguish the models for Loop I/NPS’s origin. We also note that, in both the SNRs model and GC model, at $b \gtrsim 30^\circ$, the Loop I/NPS is always a bright structure. It means that the absorption toward the high Galactic latitudes, even

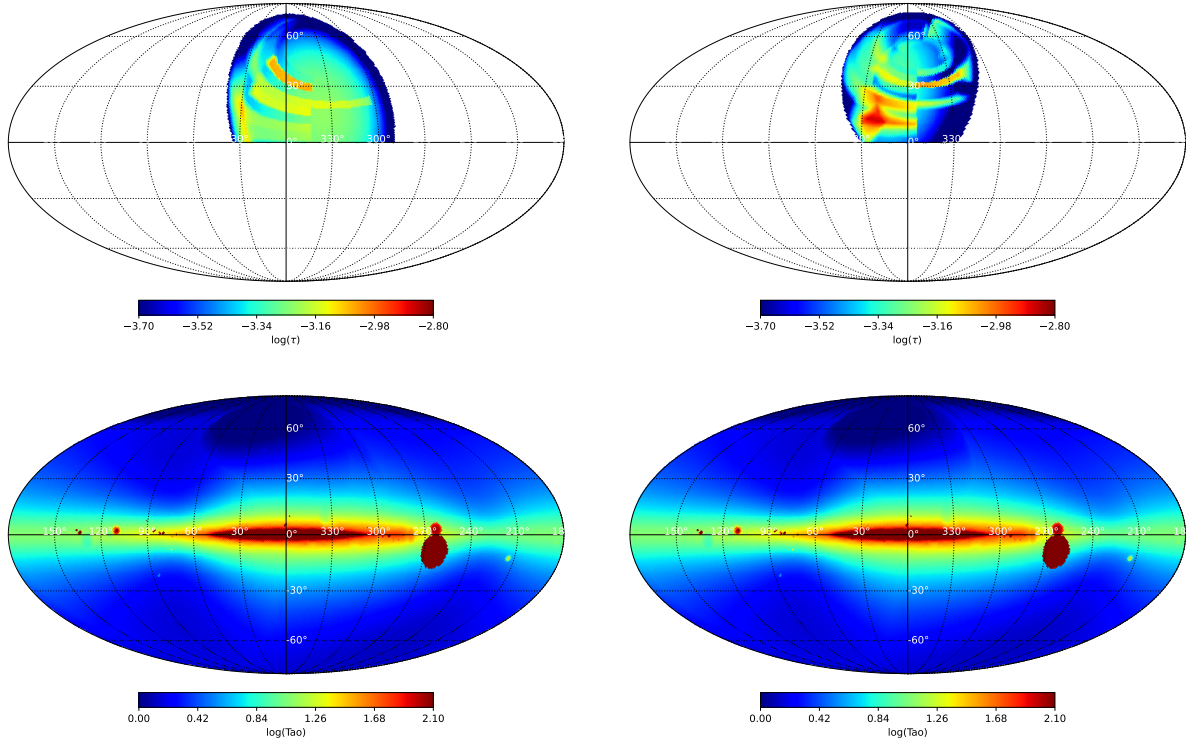


Figure 4. The free-free absorption optical depth at 1 MHz. *Left:* the optical depth of the Loop I/NPS in the shell-like SNRs model. *Right:* the optical depth in the GC model. The top panels solely show the optical depth attributed to the Loop I/NPS itself, while the bottom panels present the total absorption depth integrated over each line-of-sight.

up to above the GC, is still weak at least above 1 MHz. This is further helpful for deriving the electron distribution along the vertical (Z) direction, i.e., height of the Galactic disk.

Besides the NE2001, YMW16 is a more up-to-date Galactic electron model (Yao et al. 2017), which uses more recent data to optimize the model. YMW16 incorporates a number of local dense clumps/voids, e. g. the Gum nebula, the LHB, the Loop I/NPS, etc., but excludes those less important clumps/voids listed in NE2001. This model exhibits a higher electron density than NE2001 for the Galactic plane, Loop I and Gum nebula regions. Both models utilize a spherical shell to reconstruct the morphology of the Loop I/NPS. Our predictions for the ultra-long wavelength sky using the YMW16 electron density model are shown in Fig. 6. We have calibrated the fluctuation parameter so that the predicted global spectrum of the radio background for YMW16 is similar to that for NE2001, both consistent with observations. For YMW16, the calibrated fluctuation parameter is 0.3, while for NE2001, we basically use 3.0. The results for YMW16 are generally similar to NE2001. However, there are some differences: first, the absorption is much stronger around the Galactic plane in YMW16. Even at ~ 3 MHz, a large fraction of the regions around the Galactic plane becomes darker. Second, with YMW16 at 1 MHz, even for the SNRs model the root of the Loop I/NPS is absorbed a bit. This is because in YMW16 the Loop I/NPS itself is thick and dense, with the highest density $\sim 3 \text{ cm}^{-3}$. Third, at the Galactic plane near $l \sim 60^\circ$, there is a big and bright spot in NE2001, however, in YMW16 there is no such feature. This is because NE2001 has a giant low-density bubble in this direction, therefore the absorption is much weaker than the ambient medium. However, the primary conclusion based on both of the two models is the same: if the Loop I/NPS is a nearby object, it will be fully visible at ~ 1 MHz. However, if it is close to the GC, then only the high Galactic latitude parts at $b \gtrsim 30^\circ$ would be still visible at such low frequencies.

3.2. Discussion

We did not employ any physical hypothesis on the origin of Loop I/NPS, which is still an open question. We just adopted phenomenological models to describe its location, size, and emissivity. Our forecast on the Loop I/NPS morphology in the ultra-long wavelength band should be robust. However, we note that at different wavelengths the Loop I/NPS morphology is different. In the radio band, it is an arc above the Galactic plane; however, in the soft

X-ray band it extends to below the Galactic plane and forms dual bubbles (Predehl et al. 2020). In the polarization map, there are many spurs inside the Loop I/NPS (above and below the Galactic plane), and they are all rooted on the Galactic plane (Bennett et al. 2013; Planck Collaboration et al. 2016a; Dickinson 2018). Since our phenomenological model only aims to reproduce the observed Loop I/NPS morphology at 408 MHz, it is possible that in the ultra-long wavelength band, there are new structures near the Loop I/NPS. They may confuse our identification of the Loop I/NPS origin.

Regarding the Loop I/NPS, there are arguments supporting both a local feature and a GC feature. It is also possible that a local feature coincides with a GC feature. If the Loop I/NPS comprises two visually overlapping components, three hypotheses can be considered in this context. The first one is that the high Galactic latitude portion of Loop I/NPS is located at GC, while the remaining segment originates from a nearby source. Due to weaker absorption at high Galactic latitudes, the Loop I/NPS would still manifest as a bright, complete arc in the ultra-long wavelength band, rendering it indistinguishable from the shell-like SNRs model. The second hypothesis proposes that the high Galactic latitude portion is a nearby structure, while the remaining segment resides at the GC. Due to stronger absorption at low Galactic latitudes, only the high Galactic latitude regions are visible ultra-long wavelength band, making it indistinguishable from the GC model. The final hypothesis is an overlap of nearby and GC components throughout the Loop I/NPS. If the entire loop is observable at ultra-long wavelengths, the high-latitude section would consist of both nearby and GC components, while the low-latitude region would predominantly originate from nearby emission. This scenario may remain indistinguishable from the shell-like SNRs model.

In the 1.4 GHz polarization intensity map (Reich & Reich 2009), apparently, the low-latitude part ($b \lesssim 30 - 40^\circ$) is entirely different from higher latitudes because the Faraday depth and Faraday rotation depolarization amount become much larger (Sun et al. 2015; Dickinson 2018) at low latitudes. However, at higher frequencies (several tens of GHz), the absorption and Faraday depolarization effects are negligible even near the Galactic plane. Therefore, polarization is a more useful tool for assessing whether the high-latitude part and low-latitude part of the Loop I/NPS belong to the same structure. As if the Loop I/NPS is composed of two physically unrelated and spatially distinct components, it will be unlikely to observe a coherent polarization structure. Vidal et al. (2015) and Planck Collaboration et al. (2016a) analyzed the WMAP and Planck observations and found that in sky maps of both polarization and projected magnetic field, the entire Loop I/NPS is a coherent structure. Planck Collaboration et al. (2016a) also found that this polarization structure extends beyond the Loop I/NPS boundary. Although in a closer inspection of their projected magnetic field angle sky map (lower panel of their Fig. 20), it seems that the part close to the Galactic plane is separated from the higher latitudes part, these two parts are still difficult to disentangle.

The synchrotron spectral index could depend on the frequency (e.g. Huang et al. 2019; Cong et al. 2021; Padovani et al. 2021; Irfan et al. 2022). In Huang et al. (2019), they find the spectral index tends to become flat below ~ 20 MHz. Despite of this, in this paper, we adopt a constant spectral index for synchrotron emissivity because: 1) Currently the observations below ~ 20 MHz suffer from large uncertainties, it is a risk of extrapolating the frequency-dependence of spectral index constrained mainly by higher frequency observations to below ~ 20 MHz, and down to as low as ~ 1 MHz. 2) In the ultra-long wavelength band, the morphology of the Loop I/NPS is mainly determined by the free-free absorption (i.e., distribution of free electrons, location and geometry of the source), rather than the spectral index of synchrotron emissivity before absorption. Nevertheless, we check that, using a shallower/steeper value of β_G , or even using the frequency-dependent form (Eq. (28) of Cong et al. 2021), for synchrotron spectral index, our conclusion will not change.

The synchrotron spectral index also depends on the direction (e.g. Guzmán et al. 2011; Cong et al. 2021). In Guzmán et al. (2011) it seems that the spectra in $-130^\circ \lesssim l \lesssim 90^\circ$ are steeper, both above and below the Galactic plane. In our paper, the spectral indices of ϵ_{disk} and ϵ_L are the same. Therefore, the change of morphology other than the simple extrapolation from the power-law spectrum is attributed to the free-free absorption. However, if in the Loop I/NPS region, the dependence of spectral indices on Galactic latitudes is different from other regions, i.e., sharper at high Galactic latitudes and shallower at low Galactic latitudes, it may also result in morphology analogous to free-free absorption. However, we check that, at least above ~ 20 MHz, there is no such phenomenon, see also Guzmán et al. (2011). Moreover, both in Guzmán et al. (2011) and Cong et al. (2021), the spectra in the Loop I/NPS region, not just on the bright arc but also inside the loop, are slightly steeper. If this is true, then in the ultra-long wavelength band, the Loop I/NPS will be brighter in case the absorption is negligible. Comparatively, the absorption effects will be more conspicuous. This will strengthen our conclusion.

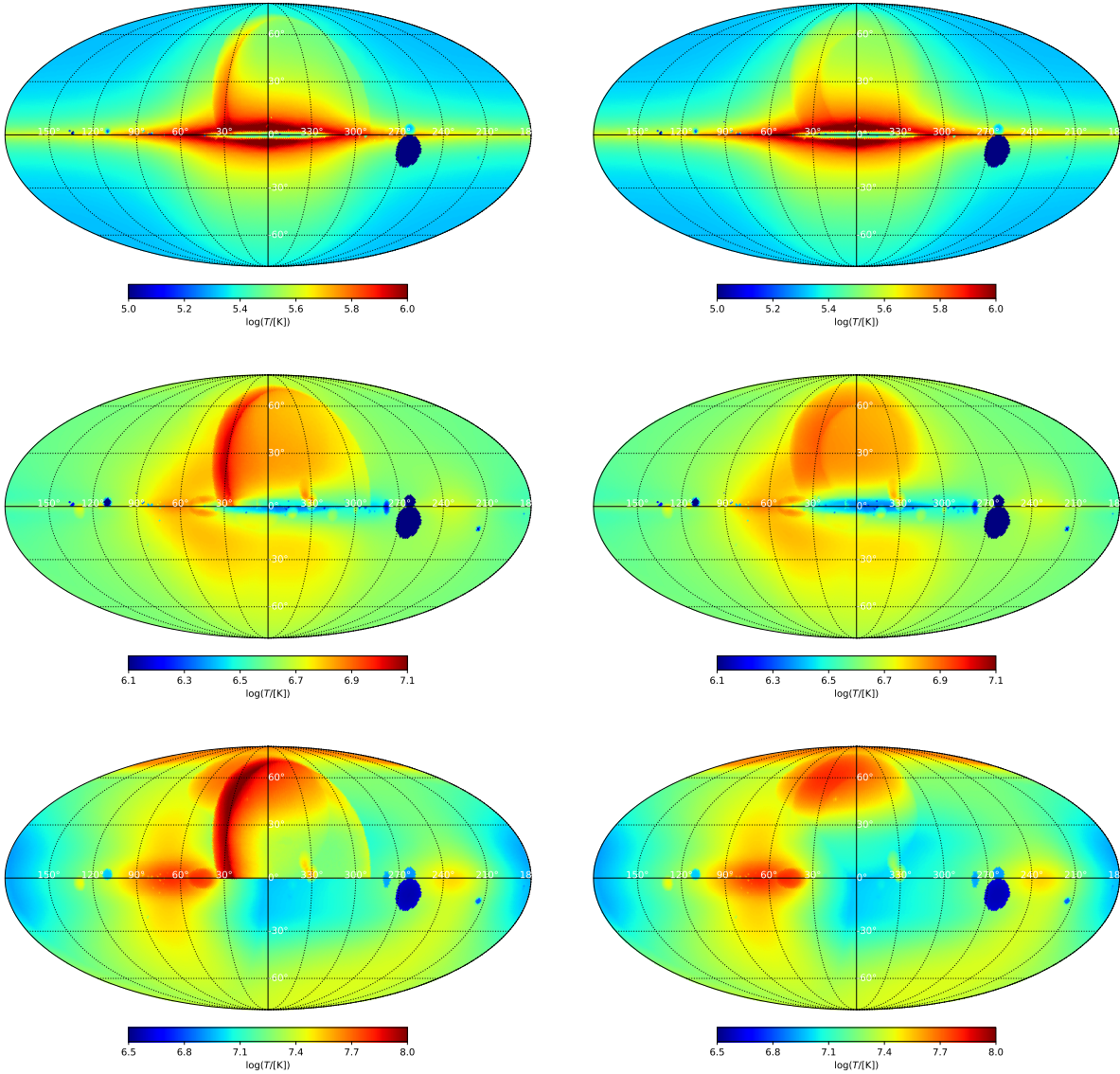


Figure 5. The predicted sky maps at frequencies 10, 3, and 1 MHz (from top to bottom) respectively, for the shell-like SNRs model of the Loop I/NPS (left column) and the GC model (right column). We use the NE2001 model for the free electron distribution. If the Loop I/NPS is a nearby object, it will still be fully visible even at ~ 1 MHz. However, if it is as far as the GC, then it vanishes at low latitudes due to absorption.

4. SUMMARY

In this paper, we investigated the Loop I/NPS structure feature in the ultra-long wavelength band. We considered two models: the shell-like SNRs model, in which the Loop I/NPS is a complex of SNRs close to our Sun, and the GC model, in which it is located close to the Galactic Center and has a large physical size. Both models can reproduce the observational feature (the loop-like feature) at high frequencies where the free-free absorption is negligible. However, the loop-like feature differs significantly in the two models in the ultra-long wavelength band where the free-free absorption is efficient ($\nu \lesssim 3$ MHz). In the shell-like SNRs model, the Loop I/NPS is still bright at frequencies as low as 1 MHz. However, in the GC model, due to the free-free absorption by the ISM between the GC and the Sun, the Loop I/NPS structure becomes dark or even fully disappears at $b \lesssim 30^\circ$. However, at high Galactic latitudes, $b \gtrsim 30^\circ$, the Loop I/NPS structure is still a notable feature in the sky. The upcoming ultra-long wavelength observations,

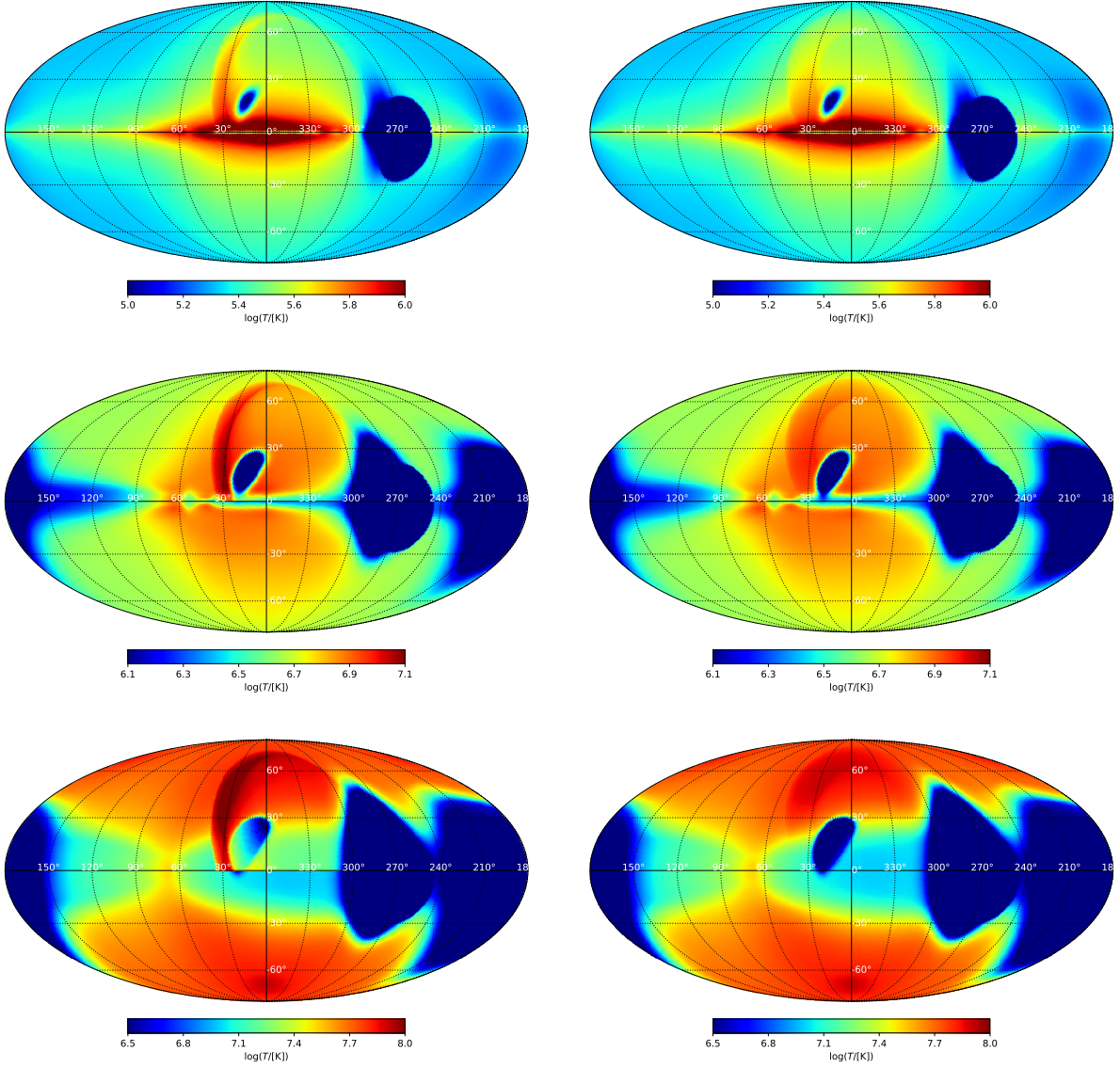


Figure 6. Similar to Fig. 5, however, the YM16 model is adopted for the electron density.

with for example the DSL (Chen et al. 2021, 2024), FAR SIDE (Burns & Hallinan 2020), etc., have the potential to distinguish these two models.

The Loop I/NPS model developed in this paper will be incorporated in the Version 2.0 of our sky model, i.e. ULSA-v2.0. We plan to make it publicly available as long as the new version is ready. Before that, the code can be obtained by making a reasonable request to the authors.

ACKNOWLEDGMENTS

We thank the anonymous referee very much for giving us detailed suggestions that greatly improve the manuscript. This work was supported by the National Key R&D Program of China No. 2022YFF0504300; National Natural Science Foundation of China (NSFC) grants 12361141814.

REFERENCES

Baldwin, J. E. 1955, MNRAS, 115, 684,
doi: [10.1093/mnras/115.6.684](https://doi.org/10.1093/mnras/115.6.684)

Bennett, C. L., Larson, D., Weiland, J. L., et al. 2013,
ApJS, 208, 20, doi: [10.1088/0067-0049/208/2/20](https://doi.org/10.1088/0067-0049/208/2/20)

- Berkhuijsen, E. M., Haslam, C. G. T., & Salter, C. J. 1971, *A&A*, 14, 252
- Borka, V. 2007, *MNRAS*, 376, 634, doi: [10.1111/j.1365-2966.2007.11499.x](https://doi.org/10.1111/j.1365-2966.2007.11499.x)
- Breitschwerdt, D., & de Avillez, M. A. 2006, *A&A*, 452, L1, doi: [10.1051/0004-6361:20064989](https://doi.org/10.1051/0004-6361:20064989)
- Burke, B. F., Graham, & Wilkinson, P. N. 2019, An introduction to radio astronomy, 4th edition (Cambridge University Press)
- Burns, J. O., & Hallinan, G. 2020, in American Astronomical Society Meeting Abstracts, Vol. 235, American Astronomical Society Meeting Abstracts #235, 130.01
- Centurion, M., & Vladilo, G. 1991, *ApJ*, 372, 494, doi: [10.1086/169995](https://doi.org/10.1086/169995)
- Chen, X., Yan, J., Deng, L., et al. 2021, *Philosophical Transactions of the Royal Society of London Series A*, 379, 20190566, doi: [10.1098/rsta.2019.0566](https://doi.org/10.1098/rsta.2019.0566)
- Chen, X., Gao, F., Wu, F., et al. 2024, arXiv e-prints, arXiv:2403.16409, doi: [10.48550/arXiv.2403.16409](https://doi.org/10.48550/arXiv.2403.16409)
- Ciotti, L., & Bertin, G. 1999, *A&A*, 352, 447, doi: [10.48550/arXiv.astro-ph/9911078](https://doi.org/10.48550/arXiv.astro-ph/9911078)
- Condon, J. J., & Ransom, S. M. 2016, Essential Radio Astronomy
- Cong, Y., Yue, B., Xu, Y., et al. 2021, *ApJ*, 914, 128, doi: [10.3847/1538-4357/abf55c](https://doi.org/10.3847/1538-4357/abf55c)
- Cong, Y., Yue, B., Xu, Y., Shi, Y., & Chen, X. 2022, *ApJ*, 940, 180, doi: [10.3847/1538-4357/ac9df7](https://doi.org/10.3847/1538-4357/ac9df7)
- Cordes, J. M., & Lazio, T. J. W. 2002, arXiv e-prints, astro. <https://arxiv.org/abs/astro-ph/0207156>
- . 2003, arXiv e-prints, astro. <https://arxiv.org/abs/astro-ph/0301598>
- Cox, D. P., & Reynolds, R. J. 1987, *ARA&A*, 25, 303, doi: [10.1146/annurev.aa.25.090187.001511](https://doi.org/10.1146/annurev.aa.25.090187.001511)
- de Geus, E. J. 1992, *A&A*, 262, 258
- Dickinson, C. 2018, *Galaxies*, 6, 56, doi: [10.3390/galaxies6020056](https://doi.org/10.3390/galaxies6020056)
- Dickinson, C., Davies, R. D., & Davis, R. J. 2003, *MNRAS*, 341, 369, doi: [10.1046/j.1365-8711.2003.06439.x](https://doi.org/10.1046/j.1365-8711.2003.06439.x)
- Dowell, J., Taylor, G. B., Schinzel, F. K., Kassim, N. E., & Stovall, K. 2017, *MNRAS*, 469, 4537, doi: [10.1093/mnras/stx1136](https://doi.org/10.1093/mnras/stx1136)
- Eastwood, M. W., Anderson, M. M., Monroe, R. M., et al. 2018, *AJ*, 156, 32, doi: [10.3847/1538-3881/aac721](https://doi.org/10.3847/1538-3881/aac721)
- Egger, R. J., & Aschenbach, B. 1995, *A&A*, 294, L25, doi: [10.48550/arXiv.astro-ph/9412086](https://doi.org/10.48550/arXiv.astro-ph/9412086)
- Foreman-Mackey, D., Hogg, D. W., Lang, D., & Goodman, J. 2013, *PASP*, 125, 306, doi: [10.1086/670067](https://doi.org/10.1086/670067)
- Guzmán, A. E., May, J., Alvarez, H., & Maeda, K. 2011, *A&A*, 525, A138, doi: [10.1051/0004-6361/200913628](https://doi.org/10.1051/0004-6361/200913628)
- Haffner, L. M., Reynolds, R. J., Tufte, S. L., et al. 2003, *ApJS*, 149, 405, doi: [10.1086/378850](https://doi.org/10.1086/378850)
- Hanbury Brown, R., Davies, R. D., & Hazard, C. 1960, *The Observatory*, 80, 191
- Haslam, C. G. T., Salter, C. J., Stoffel, H., & Wilson, W. E. 1982, *A&AS*, 47, 1
- Huang, Q., Wu, F., & Chen, X. 2019, *Science China Physics, Mechanics, and Astronomy*, 62, 989511, doi: [10.1007/s11433-018-9333-1](https://doi.org/10.1007/s11433-018-9333-1)
- Intema, H. T., Jagannathan, P., Mooley, K. P., & Frail, D. A. 2017, *A&A*, 598, A78, doi: [10.1051/0004-6361/201628536](https://doi.org/10.1051/0004-6361/201628536)
- Irfan, M. O., Bull, P., Santos, M. G., et al. 2022, *MNRAS*, 509, 4923, doi: [10.1093/mnras/stab3346](https://doi.org/10.1093/mnras/stab3346)
- Iwan, D. 1980, *ApJ*, 239, 316, doi: [10.1086/158113](https://doi.org/10.1086/158113)
- Iwashita, R., Kataoka, J., & Sofue, Y. 2023, *ApJ*, 958, 83, doi: [10.3847/1538-4357/ad0374](https://doi.org/10.3847/1538-4357/ad0374)
- Jansson, R., & Farrar, G. R. 2012, *ApJ*, 757, 14, doi: [10.1088/0004-637X/757/1/14](https://doi.org/10.1088/0004-637X/757/1/14)
- Kaaret, P., Zajczyk, A., LaRocca, D. M., et al. 2019, *ApJ*, 884, 162, doi: [10.3847/1538-4357/ab4193](https://doi.org/10.3847/1538-4357/ab4193)
- Kataoka, J., Sofue, Y., Inoue, Y., et al. 2018, *Galaxies*, 6, 27, doi: [10.3390/galaxies6010027](https://doi.org/10.3390/galaxies6010027)
- Lallemand, R. 2023, *Comptes Rendus Physique*, 23, 1, doi: [10.5802/crphys.97](https://doi.org/10.5802/crphys.97)
- Lallemand, R., Capitanio, L., Ruiz-Dern, L., et al. 2018, *A&A*, 616, A132, doi: [10.1051/0004-6361/201832832](https://doi.org/10.1051/0004-6361/201832832)
- Landecker, T. L., & Wielebinski, R. 1970, *Australian Journal of Physics Astrophysical Supplement*, 16, 1
- Large, M. I., Quigley, M. F. S., & Haslam, C. G. T. 1966, *MNRAS*, 131, 335, doi: [10.1093/mnras/131.3.335](https://doi.org/10.1093/mnras/131.3.335)
- Large, M. I., Quigley, M. J. S., & Haslam, C. G. T. 1962, *MNRAS*, 124, 405, doi: [10.1093/mnras/124.5.405](https://doi.org/10.1093/mnras/124.5.405)
- LaRocca, D. M., Kaaret, P., Kuntz, K. D., et al. 2020a, *ApJ*, 904, 54, doi: [10.3847/1538-4357/abbdff](https://doi.org/10.3847/1538-4357/abbdff)
- LaRocca, D. M., Kaaret, P., Kirchner, D. L., et al. 2020b, *Journal of Astronomical Telescopes, Instruments, and Systems*, 6, 014003, doi: [10.1117/1.JATIS.6.1.014003](https://doi.org/10.1117/1.JATIS.6.1.014003)
- Liu, T., Merloni, A., Sanders, J., et al. 2024, *ApJL*, 967, L27, doi: [10.3847/2041-8213/ad47e0](https://doi.org/10.3847/2041-8213/ad47e0)
- MacArthur, L. A., Courteau, S., & Holtzman, J. A. 2003, *ApJ*, 582, 689, doi: [10.1086/344506](https://doi.org/10.1086/344506)
- Mertsch, P., & Sarkar, S. 2013, *JCAP*, 2013, 041, doi: [10.1088/1475-7516/2013/06/041](https://doi.org/10.1088/1475-7516/2013/06/041)
- Mou, G., Wu, J., & Sofue, Y. 2023a, *A&A*, 676, L3, doi: [10.1051/0004-6361/202245401](https://doi.org/10.1051/0004-6361/202245401)
- Mou, G., Sun, D., Fang, T., et al. 2023b, *Nature Communications*, 14, 781, doi: [10.1038/s41467-023-36478-0](https://doi.org/10.1038/s41467-023-36478-0)

- Padovani, M., Bracco, A., Jelić, V., Galli, D., & Bellomi, E. 2021, *A&A*, 651, A116, doi: [10.1051/0004-6361/202140799](https://doi.org/10.1051/0004-6361/202140799)
- Panopoulou, G. V., Dickinson, C., Readhead, A. C. S., Pearson, T. J., & Peel, M. W. 2021, *ApJ*, 922, 210, doi: [10.3847/1538-4357/ac273f](https://doi.org/10.3847/1538-4357/ac273f)
- Patra, N., Subrahmanyam, R., Sethi, S., Udaya Shankar, N., & Raghunathan, A. 2015, *ApJ*, 801, 138, doi: [10.1088/0004-637X/801/2/138](https://doi.org/10.1088/0004-637X/801/2/138)
- Planck Collaboration, Ade, P. A. R., Aghanim, N., et al. 2016a, *A&A*, 594, A25, doi: [10.1051/0004-6361/201526803](https://doi.org/10.1051/0004-6361/201526803)
- Planck Collaboration, Adam, R., Ade, P. A. R., et al. 2016b, *A&A*, 594, A10, doi: [10.1051/0004-6361/201525967](https://doi.org/10.1051/0004-6361/201525967)
- Planck Collaboration, Aghanim, N., Akrami, Y., et al. 2020, *A&A*, 641, A1, doi: [10.1051/0004-6361/201833880](https://doi.org/10.1051/0004-6361/201833880)
- Predehl, P., Sunyaev, R. A., Becker, W., et al. 2020, *Nature*, 588, 227, doi: [10.1038/s41586-020-2979-0](https://doi.org/10.1038/s41586-020-2979-0)
- Quigley, M. J. S., & Haslam, C. G. T. 1965, *Nature*, 208, 741. <https://api.semanticscholar.org/CorpusID:4205652>
- Reich, P., & Reich, W. 1986, *A&AS*, 63, 205
- Reich, W., & Reich, P. 2009, in IAU Symposium, Vol. 259, *Cosmic Magnetic Fields: From Planets, to Stars and Galaxies*, ed. K. G. Strassmeier, A. G. Kosovichev, & J. E. Beckman, 603–612, doi: [10.1017/S1743921309031433](https://doi.org/10.1017/S1743921309031433)
- Reis, W., & Corradi, W. J. B. 2008, *A&A*, 486, 471, doi: [10.1051/0004-6361:20077946](https://doi.org/10.1051/0004-6361:20077946)
- Remazeilles, M., Dickinson, C., Banday, A. J., Bigot-Sazy, M. A., & Ghosh, T. 2015, *MNRAS*, 451, 4311, doi: [10.1093/mnras/stv1274](https://doi.org/10.1093/mnras/stv1274)
- Roger, R. S., Costain, C. H., Landecker, T. L., & Swerdluk, C. M. 1999, *A&AS*, 137, 7, doi: [10.1051/aas:1999239](https://doi.org/10.1051/aas:1999239)
- Sallmen, S. M., Korpela, E. J., & Yamashita, H. 2008, *ApJ*, 681, 1310, doi: [10.1086/588802](https://doi.org/10.1086/588802)
- Santos, F. P., Corradi, W., & Reis, W. 2011, *ApJ*, 728, 104, doi: [10.1088/0004-637X/728/2/104](https://doi.org/10.1088/0004-637X/728/2/104)
- Sarkar, K. C. 2019, *MNRAS*, 482, 4813, doi: [10.1093/mnras/sty2944](https://doi.org/10.1093/mnras/sty2944)
- Seiffert, M., Fixsen, D. J., Kogut, A., et al. 2011, *ApJ*, 734, 6, doi: [10.1088/0004-637X/734/1/6](https://doi.org/10.1088/0004-637X/734/1/6)
- Sersic, J. L. 1968, *Atlas de Galaxias Australes*
- Shchekinov, Y. 2018, *Galaxies*, 6, 62, doi: [10.3390/galaxies6020062](https://doi.org/10.3390/galaxies6020062)
- Sofue, Y. 1977, *A&A*, 60, 327
- . 1994, *ApJL*, 431, L91, doi: [10.1086/187480](https://doi.org/10.1086/187480)
- . 2000, *ApJ*, 540, 224, doi: [10.1086/309297](https://doi.org/10.1086/309297)
- . 2015, *MNRAS*, 447, 3824, doi: [10.1093/mnras/stu2661](https://doi.org/10.1093/mnras/stu2661)
- . 2017, *PASJ*, 69, L8, doi: [10.1093/pasj/psx067](https://doi.org/10.1093/pasj/psx067)
- Sofue, Y., Habe, A., Kataoka, J., et al. 2016, *MNRAS*, 459, 108, doi: [10.1093/mnras/stw623](https://doi.org/10.1093/mnras/stw623)
- Sofue, Y., Hamajima, K., & Fujimoto, M. 1974, *PASJ*, 26, 399
- Sofue, Y., Kataoka, J., & Iwashita, R. 2023, *MNRAS*, 524, 4212, doi: [10.1093/mnras/stad1985](https://doi.org/10.1093/mnras/stad1985)
- Su, M., Slatyer, T. R., & Finkbeiner, D. P. 2010, *ApJ*, 724, 1044, doi: [10.1088/0004-637X/724/2/1044](https://doi.org/10.1088/0004-637X/724/2/1044)
- Sun, X. H., Reich, W., Waelkens, A., & Enßlin, T. A. 2008, *A&A*, 477, 573, doi: [10.1051/0004-6361:20078671](https://doi.org/10.1051/0004-6361:20078671)
- Sun, X. H., Landecker, T. L., Gaensler, B. M., et al. 2015, *ApJ*, 811, 40, doi: [10.1088/0004-637X/811/1/40](https://doi.org/10.1088/0004-637X/811/1/40)
- Vidal, M., Dickinson, C., Davies, R. D., & Leahy, J. P. 2015, *MNRAS*, 452, 656, doi: [10.1093/mnras/stv1328](https://doi.org/10.1093/mnras/stv1328)
- Vieira, K., Korčagin, V., Carraro, G., & Lutsenko, A. 2023, *Galaxies*, 11, 77, doi: [10.3390/galaxies11030077](https://doi.org/10.3390/galaxies11030077)
- Wolleben, M. 2007, *ApJ*, 664, 349, doi: [10.1086/518711](https://doi.org/10.1086/518711)
- Yao, J. M., Manchester, R. N., & Wang, N. 2017, *ApJ*, 835, 29, doi: [10.3847/1538-4357/835/1/29](https://doi.org/10.3847/1538-4357/835/1/29)
- Zhang, H.-S., Ponti, G., Carretti, E., et al. 2024, *Nature Astronomy*, 8, 1416, doi: [10.1038/s41550-024-02362-0](https://doi.org/10.1038/s41550-024-02362-0)